Energy resolution of pulsed neutron beam provided by the ANNRI beamline at the J-PARC/MLF

K. Kino[a,*], M. Furusaka[a], F. Hiraga[a], T. Kamiyama[a], Y. Kiyanagi[a], K. Furutaka[b], S. Goko[b,1], K. Y. Hara[b], H. Harada[b], M. Harada[b], K. Hirose[b], T. Kai[b], A. Kimura[b], T. Kin[b,2], F. Kitatani[b], M. Koizumi[b], F. Maekawa[b], S. Meigo[b], S. Nakamura[b], M. Ooi[b], M. Ohta[b], M. Oshima[b], Y. Toh[b], M. Igashira[c], T. Katabuchi[c], M. Mizumoto[c], J. Hori[d]

[a]*Graduate School of Engineering, Hokkaido University, Kita 13 Nishi 8, Kita-ku, Sapporo 060-8628, Japan*

[b]*Japan Atomic Energy Agency, 2-4 Shirakata Shirane, Tokai, Naka, Ibaraki 319-1195, Japan*

[c]*Research Laboratory for Nuclear Reactors, Tokyo Institute of Technology, O-okayama, Meguro-ku, Tokyo 152-8550, Japan*

[d]*Research Reactor Institute, Kyoto University, 2-1010, Asashiro Nishi, Kumatori-cho, Sennan-gun, Osaka 590-0494, Japan*

Keywords: Pulsed neutron beam; Neutron beam line; Neutron energy resolution; Neutron capture cross section; J-PARC; MLF; JSNS; ANNRI

*Corresponding author. Tel.: +81 11 706 6703; fax.: +81 11 706 6703.
E-mail address: k-kino@eng.hokudai.jp (K. Kino).
[1]Present address: Japan Nuclear Energy Safety Organization, 4-1-28 Toranomon, Minato-ku, Tokyo 105-0001, Japan
[2]Present address: Department of Advanced Energy Engineering, Kyusyu University, Kasuga, Fukuoka 816-8580, Japan

Abstract

We studied the energy resolution of the pulsed neutron beam of the Accurate Neutron–Nucleus Reaction Measurement Instrument (ANNRI) at the Japan Proton Accelerator Research Complex/Materials and Life Science Experimental Facility (J-PARC/MLF). A simulation in the energy region from 0.7 meV to 1 MeV was performed and measurements were made at thermal (0.76–62 meV) and epithermal energies (4.8–410 eV). The neutron energy resolution of ANNRI determined by the time-of-flight technique depends on the time structure of the neutron pulse. We obtained the neutron energy resolution as a function of the neutron energy by the simulation in the two operation modes of the neutron source: double- and single-bunch modes. In double-bunch mode, the resolution deteriorates above about 10 eV because the time structure of the neutron pulse splits into two peaks. The time structures at 13 energy points from measurements in the thermal energy region agree with those of the simulation. In the epithermal energy region, the time structures at 17 energy points were obtained from measurements and agree with those of the simulation. The FWHM values of the time structures by the simulation and measurements were found to be almost consistent. In the single-bunch mode, the energy resolution is better than about 1% between 1 meV and 10 keV at a neutron source operation of 17.5 kW. These results confirm the energy resolution of the pulsed neutron beam produced by the ANNRI beamline.

1. Introduction

In recent years, intense pulsed neutron beams provided by spallation neutron sources have been used to study the neutron–nucleus reaction [1,2]. Our team has developed a new instrument, the Accurate Neutron–Nucleus Reaction Measurement Instrument (ANNRI) [3] at the Japan Spallation Neutron Source (JSNS) [4] in the Japan Proton Accelerator Research Complex/Materials and Life Science Experimental Facility (J-PARC/MLF). One of the aims of ANNRI is to provide accurate neutron capture cross-section data for minor actinides and long-lived fission products, which can be experimentally difficult to obtain for some nuclei, for example, when the amount of experimental sample is limited due to high radioactivity and/or isotopic contamination. The intense and high-quality pulsed neutron-beam of ANNRI [5] allowed successful measurement of some problematic materials [6-9].

In the measurement of neutron capture cross sections using pulsed neutron beams at ANNRI, the neutron energy is calculated from its time-of-flight (TOF) between the neutron source and experimental sample. The finite energy resolution due to the time structure of the pulsed neutron beam has to be taken into account in analyzing the experimental data. There are two factors that cause time structures for the pulsed neutron beam. One is a slowing of neutrons in the moderator of JSNS. Neutrons are generated in a mercury target through the spallation process caused by a 3 -GeV proton beam. They are then slowed down in a liquid hydrogen moderator by collisions with hydrogen. In this slowing-down process, a time structure arises in the neutron beam from the statistical nature of the collisions. The second factor is the time structure of the incident proton beam. At JSNS the incident proton beam is normally delivered in a double-bunch scheme. The time interval between the two bunches is 599 ns. For materials and life sciences, where cold or thermal neutrons are used, this scheme is not a problem since the time structure due to the slowing-down process dominates. However, for epithermal neutrons, which are used for neutron capture cross-section measurements at ANNRI, the double-bunch structure cannot be ignored.

In this paper, we present the results of studies of the time structure of the pulsed neutron beam using both simulation and measurements. The simulation covers the entire energy range for neutron capture cross-section

92 measurements. However, the simulation is based on an assumption that
93 JSNS and ANNRI work perfectly as designed. On the other hand, the
94 measurements can provide practical performance data of ANNRI, although
95 the energy range is limited.

96 **2. Simulation**

97 *2.1 Simulation procedure*

98 We performed a simulation of the neutron source using the Monte-Carlo
99 simulation code PHITS [10] to obtain the time structure of the neutron
100 beam. The procedure used in the simulation is very similar to that
101 presented in the reference [5]. We applied the nuclear data from the library
102 JENDL3 [11] to all the materials in the simulation model apart from
103 hydrogen in the moderator, for which ENDF/B-VI Release3 [12] was used.
104 The simulation model for the neutron source simulates JSNS and includes
105 the mercury target for spallation reaction, moderators, reflectors, and iron
106 shields. The parameters used for the simulation are listed in Table 1 and
107 correspond to the operational conditions of 17.5 kW. An event in the
108 simulation is initiated by the injection of a proton into the mercury target.
109 At JSNS, a 3-GeV proton beam bombards the mercury target at a repetition
110 rate of 25 Hz. In this simulation, all protons impinge on the spallation
111 target at the same starting time whereas the actual proton beam has a time
112 structure. The time structure of the proton beam was taken into account by
113 convolution after the simulation. The convolution procedure is described in
114 Section 2.2. A 100×100-mm^2 tally, which records information of particles,
115 was placed at the moderator surface perpendicular to the ANNRI beamline,
116 and neutrons passing through the tally were counted. Neutrons within a
117 very small solid angle region with respect to the ANNRI beamline were
118 considered, in order to obtain the time structure of the neutrons emitted to
119 the sample position of ANNRI.

120 [Table1 about here]

121 *2.2 Analysis of the time structures obtained by the simulation*

122 In order to represent the time structure as a function of the neutron
123 energy, we fitted time structures in many narrow neutron-energy ranges by
124 a model function. We used the model function proposed by Ikeda and
125 Carpenter [13],

126 $$\psi(v,t) = \int dt' \phi(v,t') \left[(1-R)\delta(t-t') + R\beta\theta(t-t')\exp(-\beta(t-t')) \right] \quad (t>0)$$

$$= \frac{\alpha}{2}\left\{(1-R)(\alpha t)^2 e^{-\alpha t} + 2R\frac{\alpha^2\beta}{(\alpha-\beta)^3}\left[e^{-\beta t} - e^{-\alpha t}\left(1+(\alpha-\beta)t+\frac{1}{2}(\alpha-\beta)^2 t^2\right)\right]\right\}. \quad (1)$$

Here, $\phi(v,t')$ describes the neutron flux for the slowing-down process in an infinite hydrogenous medium and is expressed as follows:

$$\phi(v,t) = \frac{\Sigma_s v}{2}(\Sigma_s v t)^2 \exp(-\Sigma_s v t) \quad (t>0),$$

Where Σ_s is the neutron macroscopic cross section and v is the velocity of neutrons. The time t was modified as $t-t_0$. The fitting parameters are t_0, α, β, R, and a scaling factor for eq. (1). Eq. (1) consists of two physical terms. One is the slowing-down term and the other is the storage term. These are $1-R$ and R in the ratio ($0 \le R \le 1$) of the total intensity, respectively. Fig. 1 shows examples of the fits. The time structures are well fitted by eq. (1) in this simulation, which uses neutrons from the coupled moderator of JSNS, although eq. (1) fails to express the time structure in the case of the decoupled moderator used for another beamline at JSNS [14]. The fitting parameters t_0, α, β, and R are plotted as a function of the neutron energy in Fig. 2. These data were fitted by polynomial functions in order to express these parameters as smooth functions of the neutron energy. A two-dimensional plot of the time structure and neutron energy is shown in Fig. 3, showing the relation between the emission time and energy of neutrons at the moderator surface. The origin of the time axis is the incident time of the proton beam on the mercury target.

[Fig. 1 about here]

[Fig. 2 about here]

[Fig. 3 about here]

The neutron time structure obtained by the simulation was convoluted with the time structure of the proton beam. At JSNS, the proton beam normally consists of two bunches separated by 599 ns. In this paper, we call this proton beam scheme the double bunch. However, depending on the JSNS operation program, the proton beam could be a single bunch. Fig. 4 shows the time structures of the proton beam during the measurements of the neutron time structures. The solid and dashed lines represent the single and double bunches, respectively. The FWHM value of each bunch is 60 ns. Three examples of the convoluted results are shown in Fig. 5. At low neutron energy (Fig. 5a), the time structures of the single and double

bunches are almost the same. However, the time structure is different for the double bunch as the neutron energy increases (Fig. 5b and 5c). Fig. 6a and 6b are two-dimensional plots, which show relations between the time structure and neutron energy. In the double-bunch mode, the time structure splits into two peaks above about 10 eV. This phenomenon reduces the energy resolution. In addition, the time structure is wider compared to that of Fig. 3 at neutron energies higher than about 10 keV because the time width of the bunch cannot be ignored compared to that of the slowing-down process in the moderator.

[Fig. 4 about here]

[Fig. 5 about here]

[Fig. 6 about here]

2.3 Simulated neutron energy resolution

We calculated the neutron energy resolution at the sample position of the Ge spectrometer at ANNRI. We used the width of the time structure in FWHM based on the results described in Section 2.2. In the case where the time structure splits into two peaks, we defined the time width as the time between the rising edge of the first peak and the falling edge of the second peak. Fig. 7 shows the time width as a function of the neutron energy. Above about 10 eV, the effect of the double bunch appears as seen in Fig. 6b. For the single bunch, the width approaches about 60 ns as the neutron energy increases. This reflects the width of the proton beam bunch. On the other hand, for the double bunch, the width approaches about 600 ns, reflecting the time distance between the two bunches. In the TOF technique, the uncertainty in neutron energy ΔE is calculated from the difference in energies at $t+\Delta t$ and $t-\Delta t$. Here, t is the TOF between the moderator and experimental sample. If Δt is small compared to t, the energy resolution $\frac{\Delta E}{E}$ is related to the time resolution $\frac{\Delta t}{t}$ by the following equation:

$$\frac{\Delta E}{E} = 2\frac{\Delta t}{t}.$$

For the Ge spectrometer at ANNRI, the TOF distance is 21.5 m. By using the values of the width in Fig. 7 as Δt, we obtained the energy resolution shown in Fig. 8. For the single bunch, the energy resolution is about 1% or less between 1 meV and 10 keV. For the double bunch, the resolution

193 decreases above 10 eV and is 10 times less than that of the single bunch
194 above about 10 keV.
195 [Fig. 7 about here]
196 [Fig. 8 about here]
197 **3. Measurements**
198 *3.1 Thermal neutron*
199 We measured the time structures of the neutron beam based on the
200 thermal neutron energy. The measurement set up is shown in Fig. 9. We
201 placed a mica sample with dimensions of 50×50 mm^2 and a thickness of 5
202 mm in the beamline, 28.5 m from the moderator. Mica is a silicate mineral
203 and has a layered crystal structure. We used a mica sample with a layer
204 interval of 10.4 Å. Diffracted neutrons from the sample were detected by a
205 helium-3 proportional counter at an angle of 162 degrees with respect to the
206 beamline downstream and a distance of 650 mm from the sample. TOF
207 spectra of the diffracted neutrons were obtained. The proton beam had a
208 repetition rate of 25 Hz and a double-bunch structure. The JSNS power was
209 120 kW.
210 From the Bragg's law, the interval d, scattering angle θ, and neutron
211 wavelength λ are related as follows:
212 $$\lambda = 2d\sin(\theta). \quad (2)$$
213 If the product of the wavelength of the incident neutron and a positive
214 integer value n is equal to the wavelength λ in eq. (2), diffraction occurs.
215 The diffraction peaks in the TOF spectra reflect the time structure of the
216 neutron beam. Figs. 10a and 10b show the TOF spectra under two
217 conditions: the disk chopper, which cuts the frame overlap, was not used for
218 Fig. 10a and used for 10b. The arrows in these figures indicate the expected
219 positions of the diffraction peaks. The numbers above some of the arrows
220 correspond to the value n. The n=2 and 3 diffraction peaks in Fig. 10a
221 appear in the second frame. The intensities of the diffraction peaks in Fig.
222 10b are lower than those in Fig. 10a because we had to increase the neutron
223 counter's discriminator threshold due to noise from the disk chopper. The
224 spectra with no peaks in these figures, represent the background, measured
225 by setting the angle of the mica sample off the diffraction condition. The
226 background was subtracted from the foreground spectra. We obtained
227 sufficient statistics to analyze the diffraction peaks with n=2, 3, 4, 5, 6, 8, 9,
228 10, 11, 12, 13, 14, and 18. Fig. 11 shows comparisons of these diffraction

peaks with the time structures obtained by the simulation. The minimum and maximum neutron energies for the diffractions are 0.76 and 62 meV, respectively. The value indicated in each figure corresponds to the neutron energy of the diffraction. The double bunch does not affect the measurements for thermal neutron energies, as shown in Fig. 6. In Fig. 11, the intensities for the simulation data are scaled to those of the measurement data. All the figures show good agreement between the measurement and simulation in the intensity range from two to three orders of magnitudes. In addition, both the components of eq. (1) show agreement between the measurement and simulation. This result indicates that JSNS and the ANNRI beamline work properly for the thermal neutron energies.

[Fig. 9 about here]

[Fig. 10 about here]

[Fig. 11 about here]

The measured diffraction peaks were fitted using eq. (1) to get the FWHM values of the time structures to allow a comparison with simulation. All the parameters for the neutron time structure described in section 2.2 were free during the fitting process. In the thermal energy region, the time structure of the proton beam is negligible. Fig. 12 shows examples of the fits. The experimental data are well fitted by eq. (1). Fig. 13 compares the experimentally obtained parameters α, β, and R with those in Fig. 2. Both sets of parameters are in agreement.

[Fig. 12 about here]

[Fig. 13 about here]

3.2 Epithermal neutron

For epithermal neutrons, we used the resonances of the neutron capture reaction for tantalum-181. The measurement setup is shown in Fig. 14. We placed a tantalum foil with an area of 100×100 mm^2 and a thickness of 0.1 or 0.01 mm in the beamline, 29.54 m from the moderator. Prompt gamma rays were emitted immediately following the neutron capture reaction. The difference between the time of incidence of the proton beam on the mercury target of the JSNS and the time that prompt gamma rays are detected enables us to measure the neutron TOF. The time structure of the neutron beam is convoluted with the TOF spectrum and can be extracted from the measured TOF spectra for neutron capture resonances. We detected the

prompt gamma rays by a scintillation detector. The detector consists of three sets of plastic scintillator and photomultiplier tube. The scintillators were 703 cm^3 in volume in total and were set at about 100 mm from the beamline in a direction normal to the beamline. The detection efficiency for gamma rays by a plastic scintillator is generally low. However, a plastic scintillator is very insensitive to background neutrons because the cross section of the capture reactions for light nuclei in the plastic scintillator is small. We simulated the neutron background coming from the tantalum foil and found that it was negligible for the analyzed resonances. The threshold level for the signal processing of the detector was set to 1 MeV for gamma rays, taking into account the need for sufficient statistics and background rejection.

[Fig. 14 about here]

We took two data sets with two tantalum foils, one thick (0.1 mm) and one thin (0.01 mm). The data for the thick foil is for the higher energy resonances, whose cross section is small. This data was taken in the single-bunch operation mode of JSNS. The data for the thin foil is for the low energy resonances. For the low energy resonances, the TOF spectrum with the thick tantalum foil saturates at the peak of the resonance due to its large cross section. The operation of JSNS was the double bunch for the data with the thin foil.

The measured TOF spectrum with the thick foil overlapped the TOF spectrum of the evaluated cross section at a temperature of 300 K in the nuclear data library JENDL-3.3 [11] in Fig. 15. As seen in this figure, we observed resonance peaks of Ta-181 at neutron energies from 4.3 eV up to about 400 eV.

[Fig. 15 about here]

We extracted the time structures of neutron pulses from the measured TOF spectra using the following procedure. First, we obtained the neutron pulses by a convolution of the time structure modeled by eq. (1) and the time structure of the proton beam. Second, the neutron pulses were convoluted with the TOF spectra of neutron capture resonances, which are expressed by the single-level Breit–Wigner equation. The resonance parameters used in the single-level Breit–Wigner equation were those in JENDL-3.3. Here, we took into account the Doppler effect on resonances using the technique of effective temperature [15]. Finally, we fitted the TOF spectra obtained as

explained above to the measured spectra. All of the parameters for the neutron time structure described in section 2.2 were free during the fitting process. Among the many resonances, we chose isolated ones, namely the resonance with the least overlap with neighboring resonances. Fig. 16 shows examples of fits for the resonances of energies 4.28, 20.29, and 208.48 eV. In Figs. 16a and 16b, the spectra have symmetrical shapes because the time structure of the neutron pulses is narrow compared to the resonance width, and the Doppler broadening affects the TOF spectra symmetrically for Ta-181 resonances at room temperature. On the other hand, the spectrum in Fig. 16c shows an asymmetrical shape, which reflects the time structure of the neutron pulses. Fig. 16 also shows the resonances calculated using the parameters in Fig. 2. The resonance shapes were well reproduced by the simulation. Fig. 17 compares the experimentally obtained parameters α, β, and R with those in Fig. 2. Both sets of parameters are in agreement.

The FWHM values of the neutron pulses for single-bunch mode were obtained. We used the TOF spectrum with the tantalum foil of thickness of 0.1 mm for all the resonances except the 4.28 and 10.36 eV resonances, for which the double-bunch structure of the proton beam was taken into account for fitting.

[Fig. 16 about here]

[Fig. 17 about here]

4. Comparison of the simulation and measurements

We compared the time structures of the neutron pulses between the simulation and measurements. Fig. 18 shows the FWHM values corresponding to those of the single bunch. The error bar for each point, which originates from the statistical uncertainty of the measurement spectrum, is within the size of the marker. The trend and absolute values of the measurement results are almost reproduced by the simulation. This result implies that JSNS and the ANNRI beamline work properly and the simulation is reliable for deducing the FWHM values in the energy regions where the measurements data were not obtained.

[Fig. 18 about here]

5. Conclusions

We have performed a simulation and performed measurements of the time structure of the neutron pulses at the ANNRI beamline, to obtain

accurate data of the neutron-capture cross-sections for minor actinides and long-lived fission products.

The simulation, which models the neutron source precisely, predicted the time structure for neutron energies between 0.7 meV and 1 MeV. From this we obtained the energy resolution that is determined by the TOF technique. For the double-bunch mode, the energy resolution was found to deteriorate above about 10 eV, demonstrating that we need a special method to analyze experimental data at high energy resolution. We made measurements in the thermal and epithermal energy regions with different methods. In the thermal energy region, time structures at 13 energy points were measured using diffraction by a mica sample. The shapes of the time structures were in agreement with those of the simulation predictions. In the epithermal energy region, we obtained the TOF spectra for neutron capture resonances by tantalum-181 nuclei. From these spectra, we extracted time structures at 17 energy points.

The FWHM values of the time structures of the neutron pulses for both the simulation and measurement data were in good agreement with regard to the trend and the absolute value. This result shows that the neutron source and ANNRI beamline are working properly, and the reliability of the simulation is also confirmed. In single-bunch mode, we found that the energy resolution was better than about 1% in the energy region from 1 meV to 10 keV.

Currently, the power of JSNS is increasing and will reach 1 MW in the near future. The properties of the proton beam, such as the time width of the beam bunch and the spatial distribution on the mercury target, may change with the increase in power. Therefore, it is important to periodically check the time structure of the neutron pulses by simulation and measurement.

Acknowledgments

Present study is the result of “Study on nuclear data by using a high intensity pulsed neutron source for advanced nuclear system” entrusted to Hokkaido University by the Ministry of Education, Culture, Sports, Science, and Technology of Japan (MEXT). This work was supported by JSPS KAKENHI Grant Number 22226016.

References

[1] C. Guerrero, et al., Nucl. Instrum. Methods. Phys. Res. A 608 (2009) 424.
[2] R. Reifarth, et al., Nucl. Instrum. Methods. Phys. Res. B 241 (2005) 176.
[3] M. Igashira, Y. Kiyanagi, M. Oshima, Nucl. Instrum. Methods. Phys. Res. A 600 (2009) 332.
[4] Y. Ikeda, Nucl. Instrum. Methods. Phys. Res. A 600 (2009) 1.
[5] K. Kino, et al., Nucl. Instrum. Methods. Phys. Res. A 626 (2011) 58.
[6] S. Goko, et al., J. Nucl. Sci. Technol. 47 (2010) 1097.
[7] A. Kimura, et al., J. Nucl. Sci. Technol. 49 (2012) 708.
[8] J. Hori, et al., J. Korean Phys. Soc. 59 (2011) 1777.
[9] S. Nakamura, et al., J. Korean Phys. Soc. 59 (2011) 1773.
[10] K. Niita, N. Matsuda, Y. Iwamoto, H. Iwase, T. Sato, H. Nakashima, Y. Sakamoto and L. Sihver, PHITS: Particle and Heavy Ion Transport code System, Version 2.23, JAEA-Data/Code 2010-022 (2010).
[11] K. Shibata, et al., J. Nucl. Sci. Technol. 39 (2002) 1125.
[12] R. E. Macfarlene, “Cold-Moderator Scattering Kernel Methods”, LA-UR-98-655, Los Alamos National Laboratory, (1998).
[13] S. Ikeda and J. M. Carpenter, Nucl. Instr. and Meth. A 239 (1985) 536.
[14] M. Harada, N. Watanabe, F. Maekawa, M. Futakawa, Nucl. Instr. and Meth. Phys. Res. A 597 (2008) 242.
[15] Y. Kiyanagi, et al., J. Nucl. Sci. Technol. 42 (2005) 263.

Figure captions

Figure 1

Examples of fits of eq. (1) to the time structures of neutron pulses obtained by the simulation. The solid lines represent eq. (1). The dashed and dotted lines correspond to the slowing-down and storage terms in eq. (1), respectively. The values indicated in the figures are neutron energies.

Figure 2

Fit parameters t_0, α, β, and R. The solid lines are polynomial functions, which were fitted to the data points.

Figure 3

Two-dimensional plot of the time and energy of neutrons at the moderator surface. The time structure of the proton beam is not convoluted. The intensity is normalized at the pulse peak. This plot is drawn at 1/100th of the intensity of the peak.

Figure 4

Time structures of the proton beam for the JSNS operation conditions when the measurements were performed. The solid and dashed lines represent the single-bunch and double-bunch modes, respectively. The FWHM value of each bunch is 60 ns.

Figure 5

Examples of convolution of the time structure originating from the slowing-down process in the moderator with the proton-beam time structure. The neutron energies of figs a, b, and c are 1.02 meV, 40.7 eV, and 1.02 keV, respectively. The solid and dotted lines are the results for the double- and single-bunch modes, respectively.

Figure 6

Two-dimensional plots of the time and energy of neutrons at the moderator surface. The time structure of the proton beam is taken into account. Figures a and b are the results for the single- and double-bunch modes, respectively.

Figure 7

The FWHM values for the time structure by the simulation as a function of neutron energy. The solid and dashed lines represent the single- and double-bunch modes, respectively.

Figure 8

Neutron energy resolution at 21.5 m from the moderator based on the simulation. The solid and dashed lines represent the single- and double-bunch modes, respectively.

Figure 9

Measurement setup for the time structure of neutron pulses at thermal neutron energies.

Figure 10

TOF spectra obtained by the diffraction method. The disk chopper was not operated for figure a and was operated for figure b. The spectra, with no peaks are the background data, which were taken by setting the angle of the mica sample off the diffraction condition. The arrows in these figures indicate the expected positions of the diffraction peaks. The numbers above some of the arrows correspond to the parameter n, as explained in the text.

Figure 11

Comparison of measured diffractions (data points) with the time structures obtained by the simulation (solid lines). The value indicated in each figure corresponds to the neutron energy of the diffraction. The dashed and dotted lines are the slowing-down and storage terms in eq. (1), respectively.

Figure 12

Examples of fits of the measured data with eq. (1). The solid lines represent the fitting results. The dashed and dotted lines are the slowing-down and storage terms in eq. (1), respectively.

Figure 13

Comparison of parameters α, β, and R in the thermal neutron region. The lines and data points are the simulation and measurement data, respectively.

Figure 14

Measurement setup for the time structure of neutron pulses in the epithermal neutron energy region.

Figure 15

Measured TOF spectrum with the thick tantalum foil and the cross section of the neutron capture reaction based on the nuclear data library JENDL-3.3 at a temperature of 300 K.

Figure 16

Examples of fits of the measured TOF spectra in the epithermal neutron energy region. Figures a, b, and c show the resonances with energies of 4.28, 20.29, and 208.48 eV, respectively. Resonance curves are also evident, which are calculated using the parameters obtained by the simulation.

Figure 17

Comparison of parameters α, β, and R in the epithermal neutron region. The lines and data points are the simulation and measurement data, respectively.

Figure 18

Comparison between the simulation and measurements of the FWHM values of the time structures of neutron pulses for single-pulse mode.

Table 1

Parameters used in the simulation of the neutron source.

Proton beam	Energy	3 GeV
	Spatial shape	Rectangle (uniform distribution)
		−25.9 − +25.9 mm (horizontal)
		−12.6 − +12.6 mm (vertical)
Liq.H_2 moderator	Temperature	19.7 K
	Density	4.2655×10^{22} atoms/cm^3
	Ortho-Para ratio	Para 100%
Cooling water	Reflector	Light water
	Mercury target	Light water

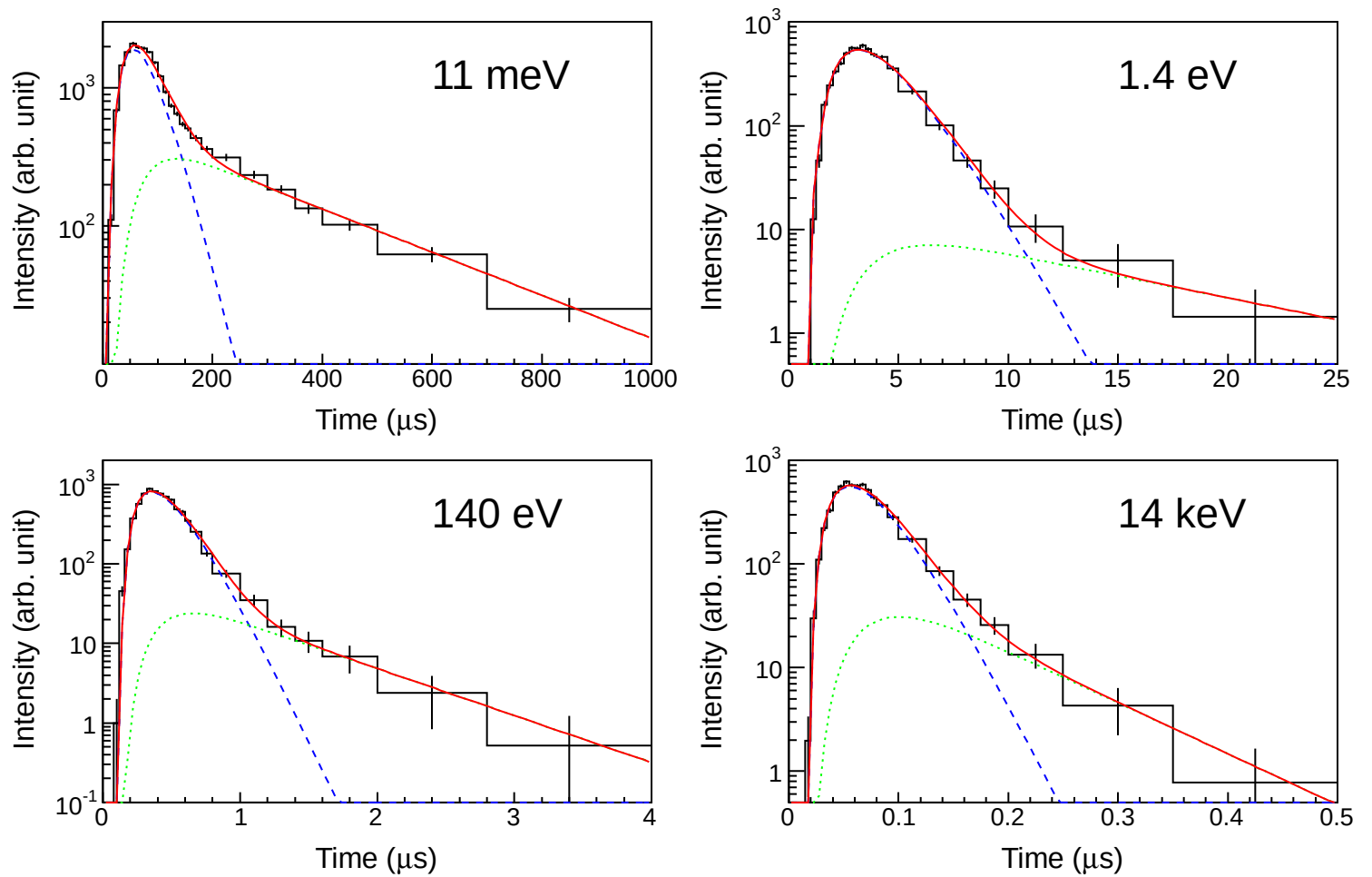
11 meV
1.4 eV
140 eV
14 keV
Intensity (arb. unit)
Time (μs)

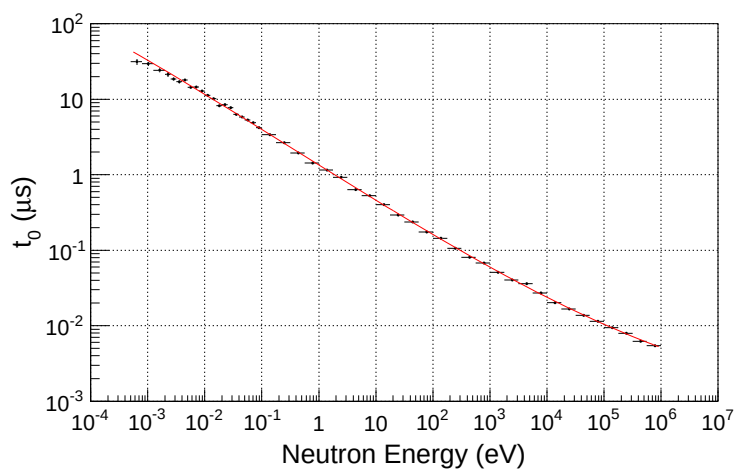
t_0 (μs)
Neutron Energy (eV)

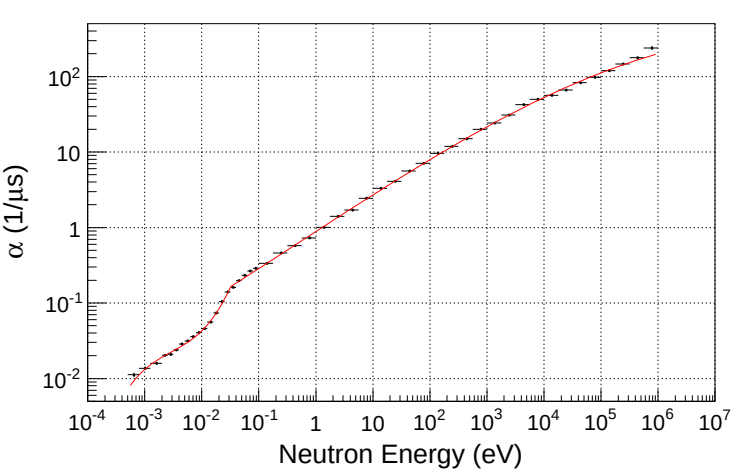
α (1/μs)
Neutron Energy (eV)

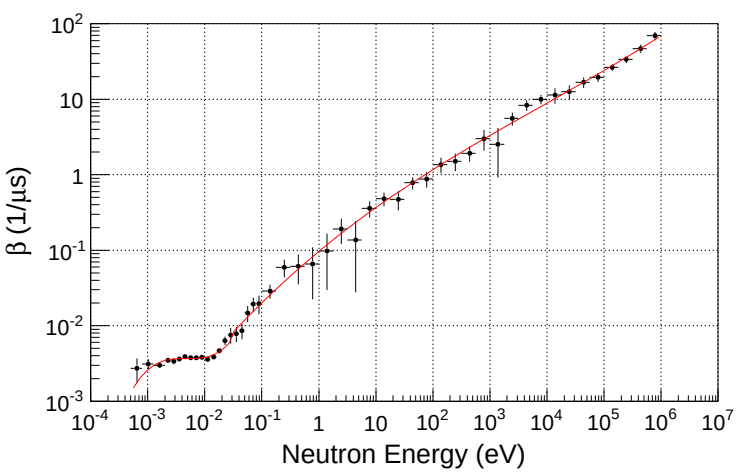
β (1/μs)
Neutron Energy (eV)

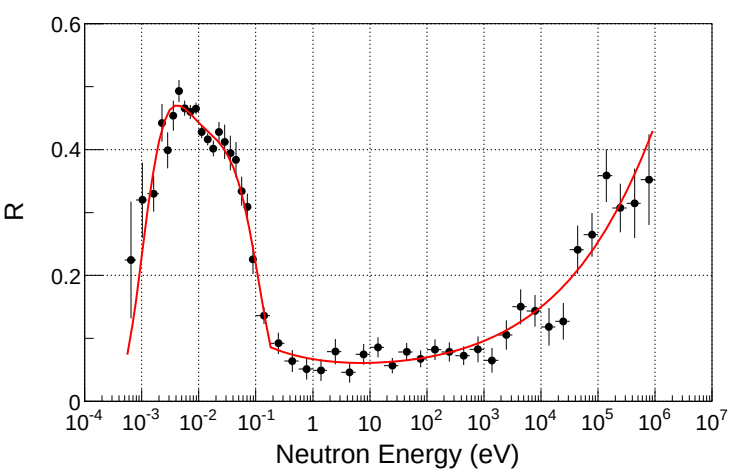
R
Neutron Energy (eV)

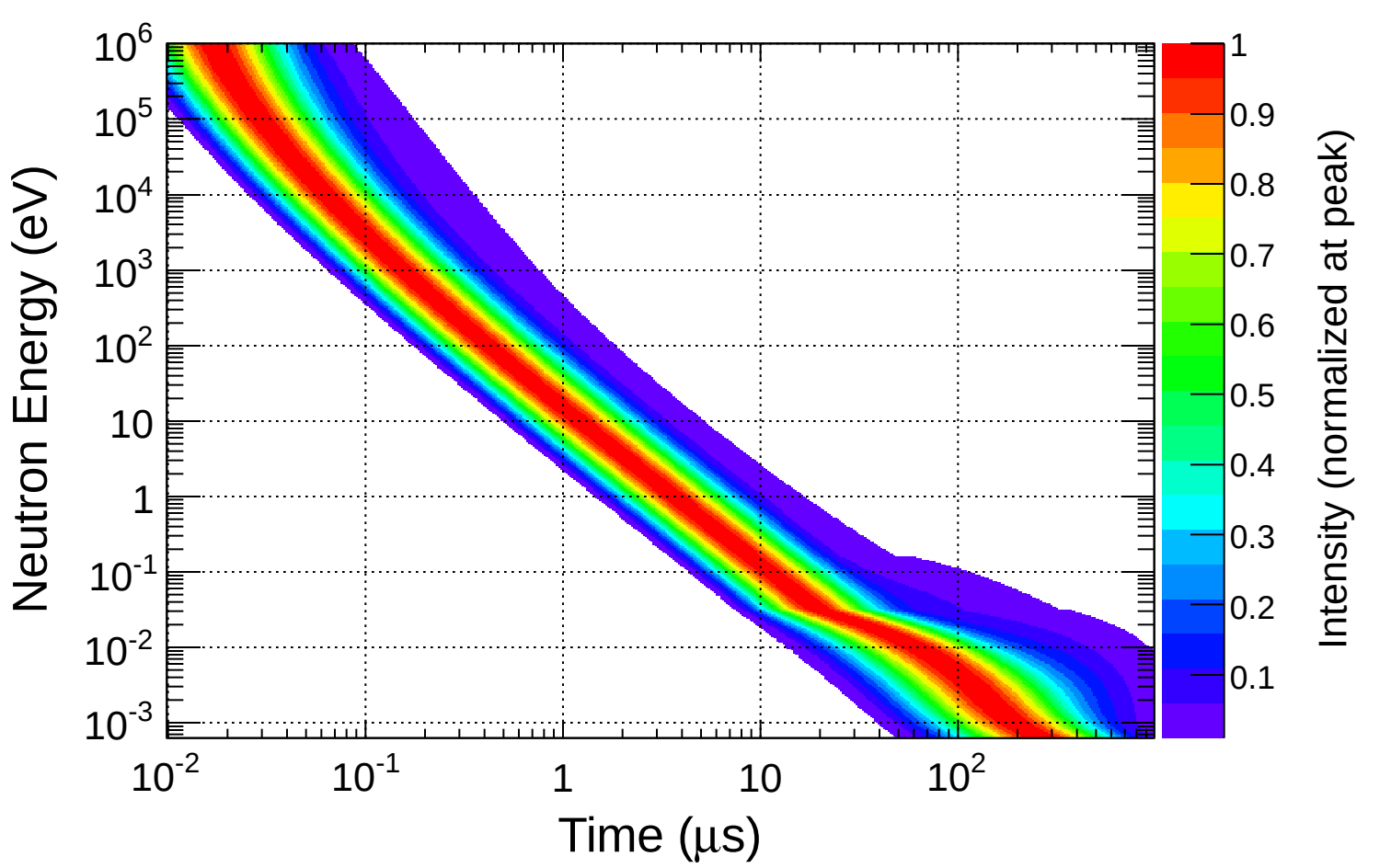
Neutron Energy (eV)
10^{6}
10^{5}
10^{4}
10^{3}
10^{2}
10
1
10^{-1}
10^{-2}
10^{-3}
10^{-2}
10^{-1}
1
10
10^{2}
Time (μs)
Intensity (normalized at peak)
1
0.9
0.8
0.7
0.6
0.5
0.4
0.3
0.2
0.1

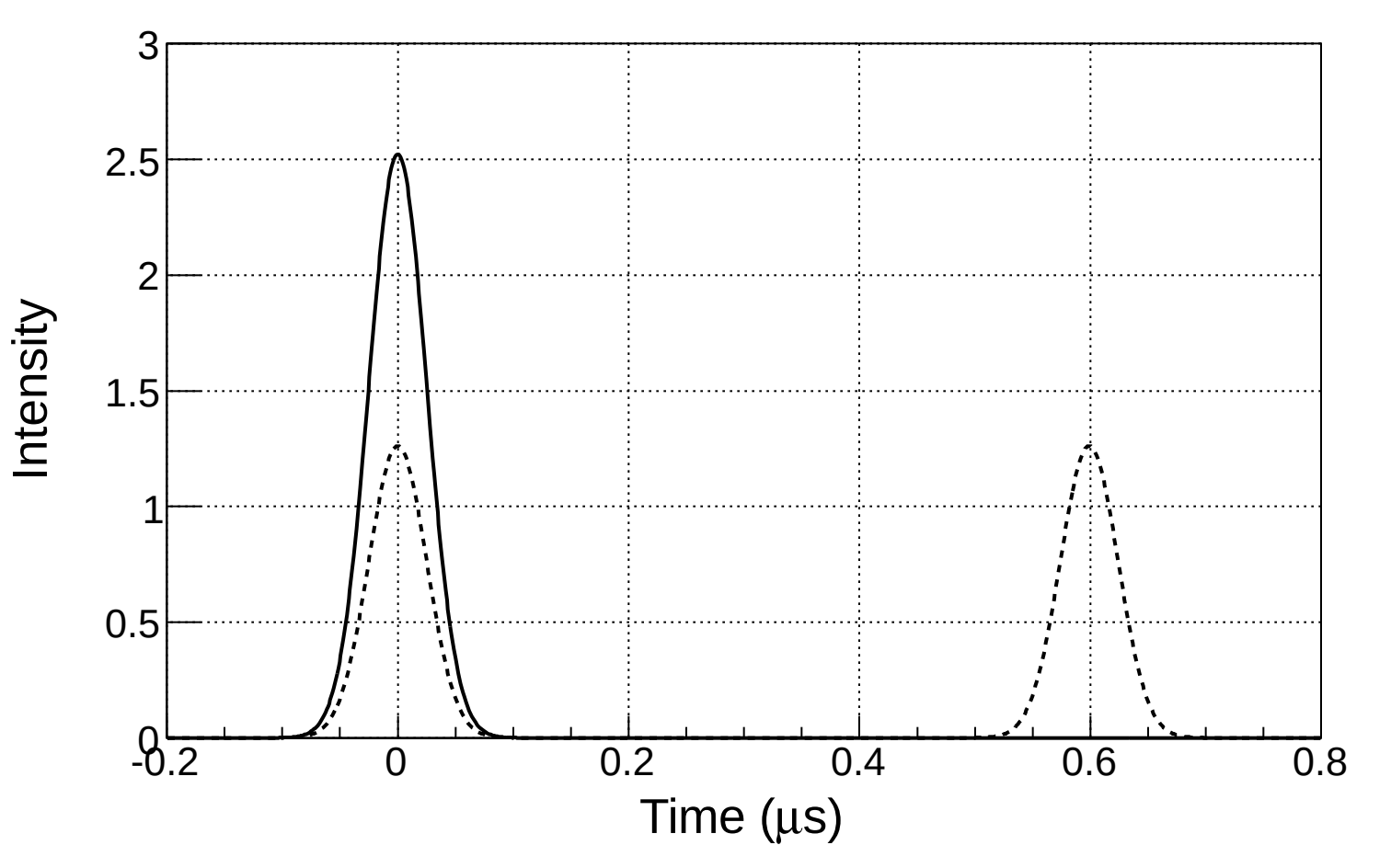
Intensity
Time (μs)
3
2.5
2
1.5
1
0.5
0
-0.2
0
0.2
0.4
0.6
0.8

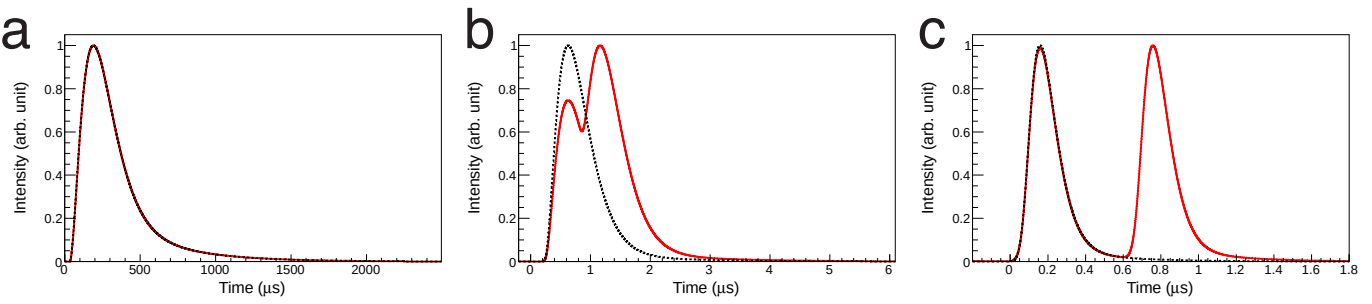
a
Intensity (arb. unit)
Time (μs)
b
Intensity (arb. unit)
Time (μs)
c
Intensity (arb. unit)
Time (μs)

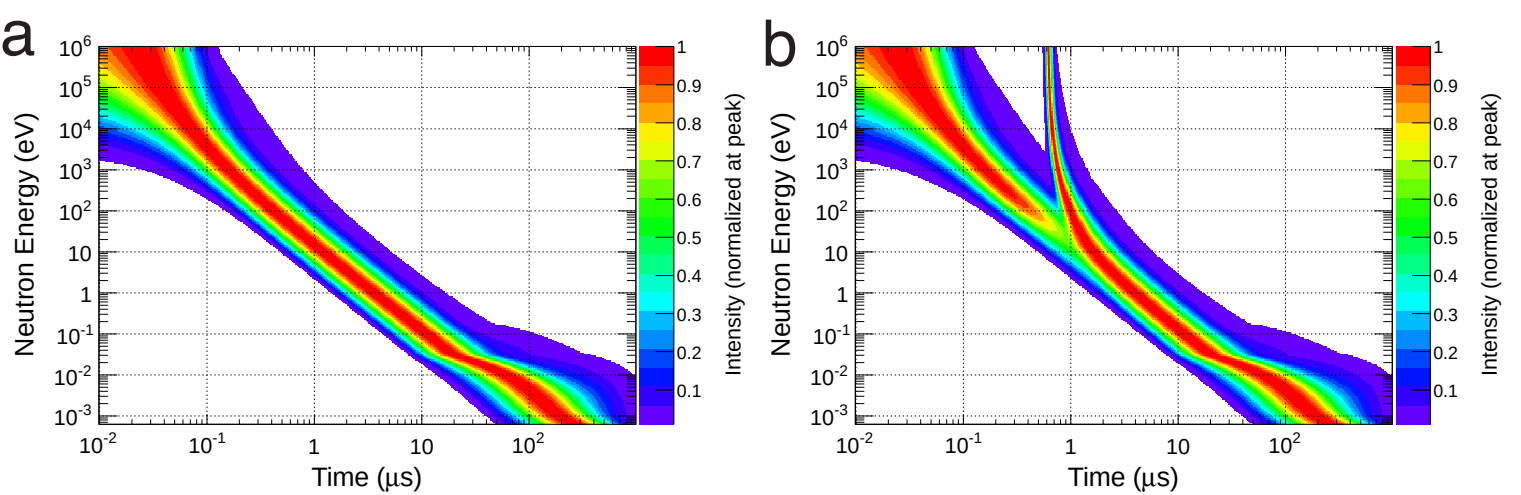
a
b
Neutron Energy (eV)
Time (μs)
Intensity (normalized at peak)
10^{6}
10^{5}
10^{4}
10^{3}
10^{2}
10
1
10^{-1}
10^{-2}
10^{-3}
10^{-2}
10^{-1}
1
10
10^{2}
1
0.9
0.8
0.7
0.6
0.5
0.4
0.3
0.2
0.1

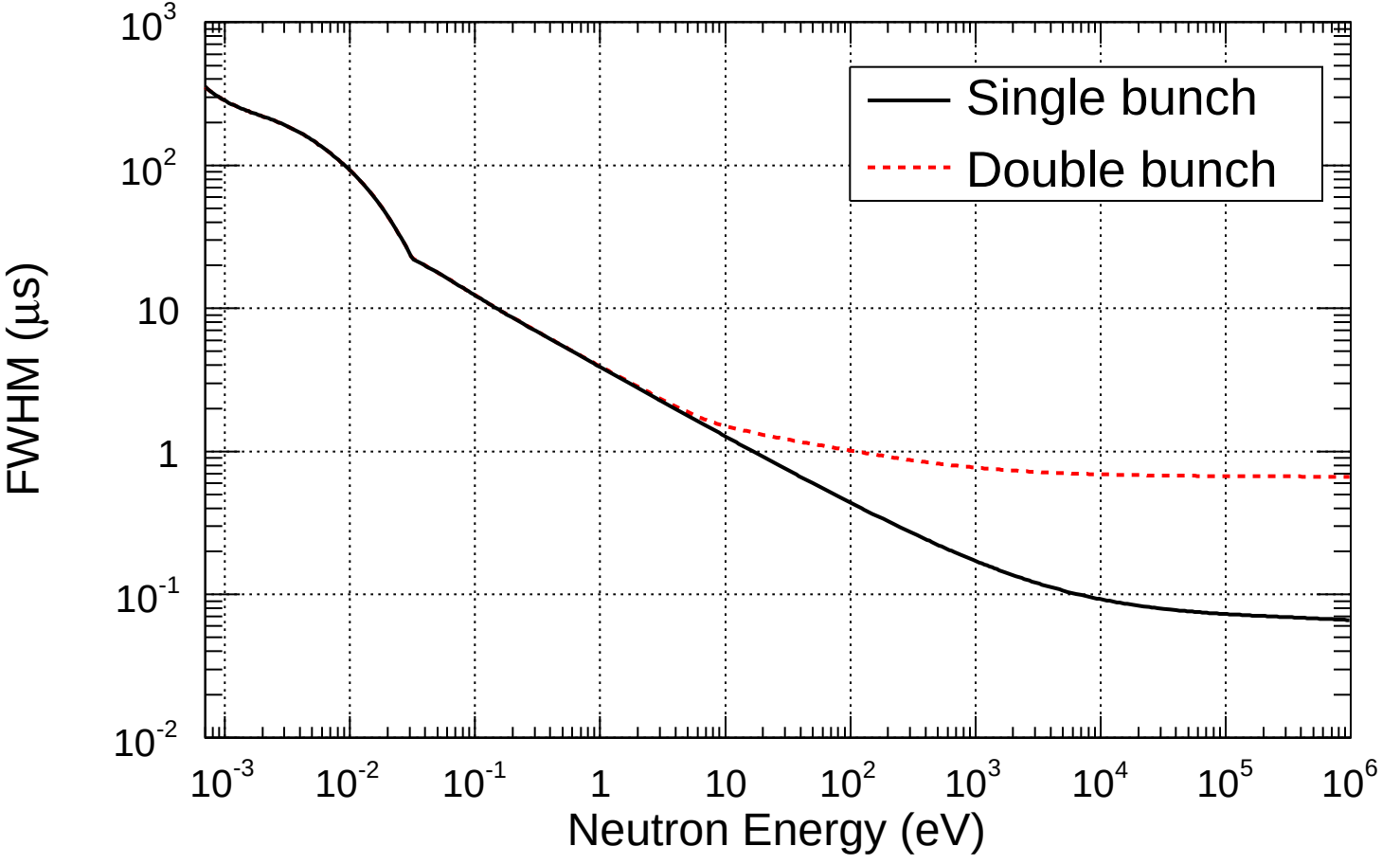
Single bunch
Double bunch
FWHM (μs)
Neutron Energy (eV)
10^3
10^2
10
1
10^-1
10^-2
10^-3
10^-2
10^-1
1
10
10^2
10^3
10^4
10^5
10^6

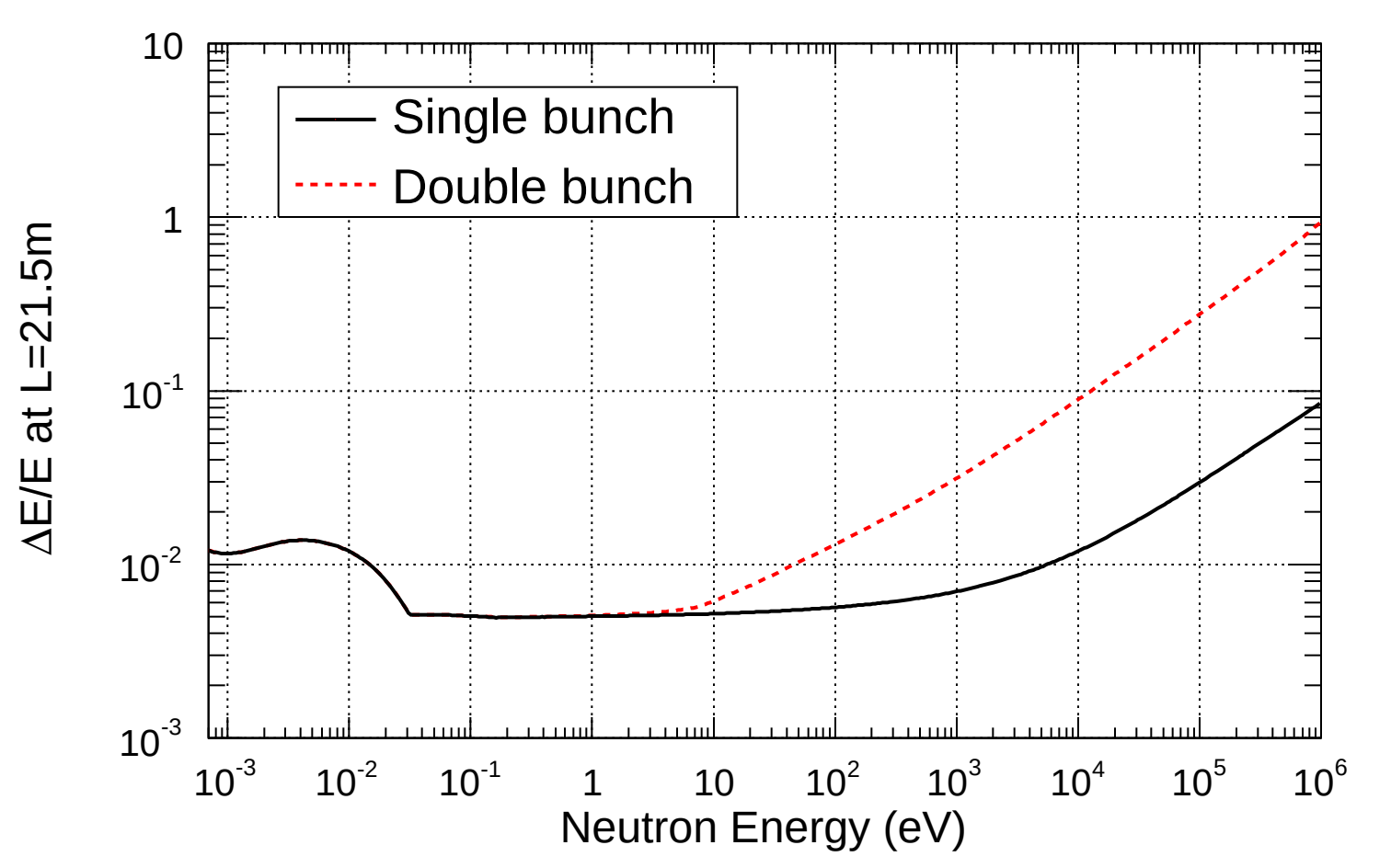
Single bunch
Double bunch
ΔE/E at L=21.5m
Neutron Energy (eV)
10
1
10-1
10-2
10-3
10-3
10-2
10-1
1
10
102
103
104
105
106

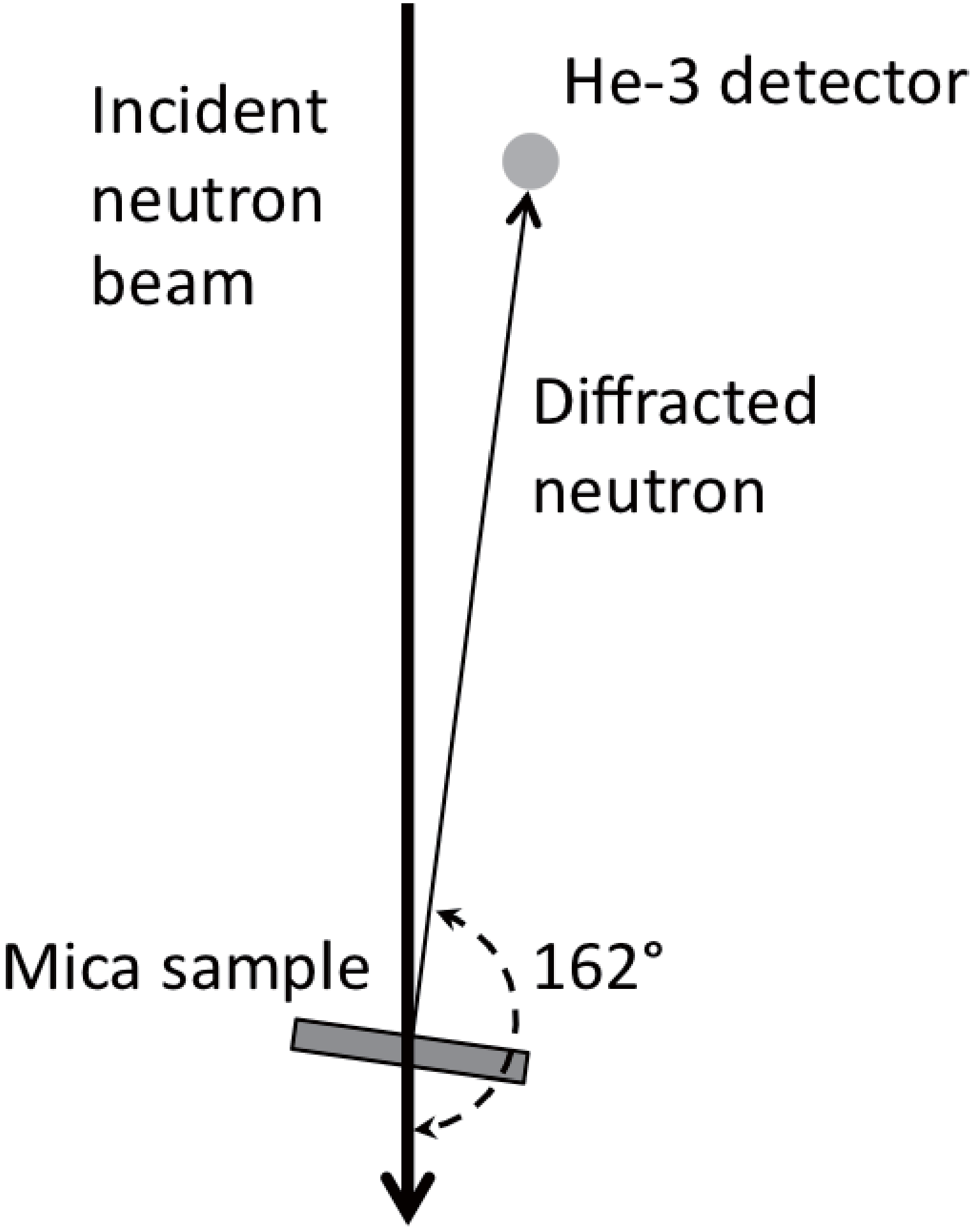
Incident
neutron
beam
He-3 detector
Diffracted
neutron
Mica sample
162°

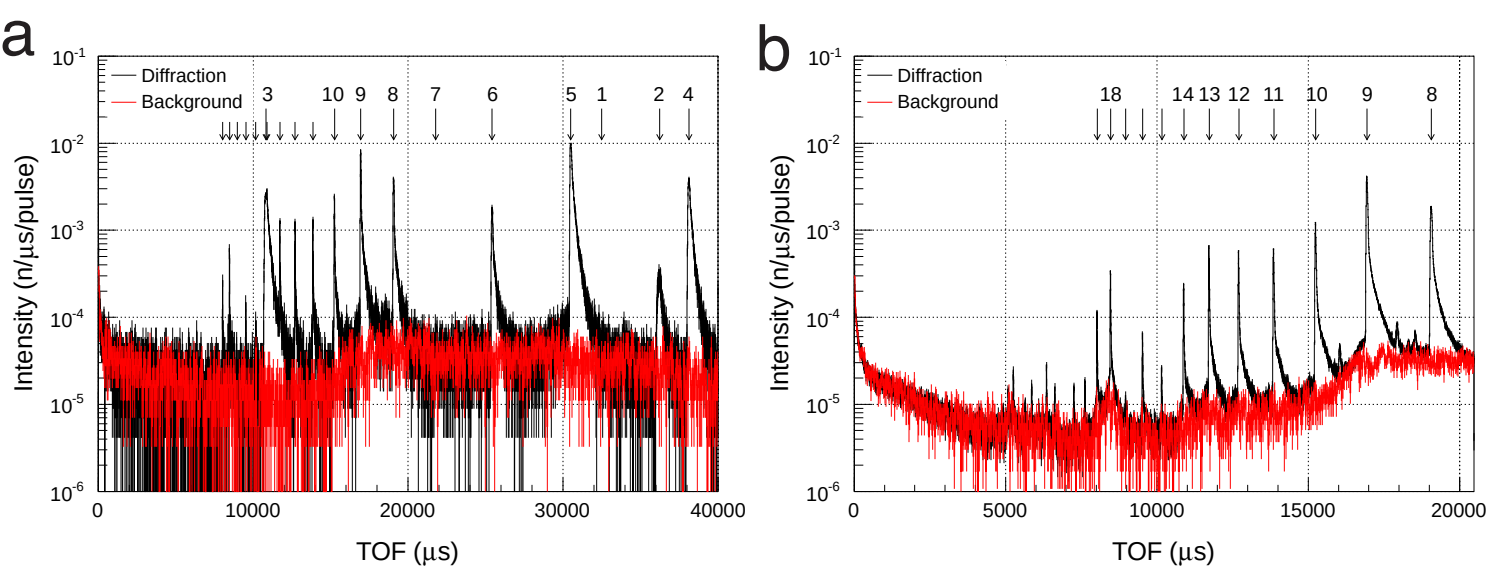
a
Diffraction
Background
3
10
9
8
7
6
5
1
2
4
Intensity (n/μs/pulse)
TOF (μs)
b
Diffraction
Background
18
14
13
12
11
10
9
8
Intensity (n/μs/pulse)
TOF (μs)

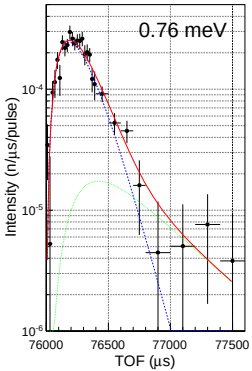
0.76 meV
Intensity (n/μs/pulse)
TOF (μs)

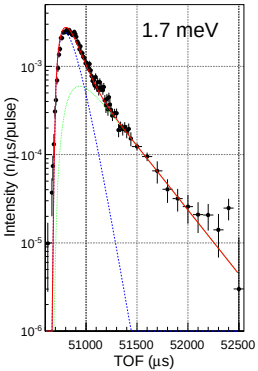
1.7 meV
Intensity (n/μs/pulse)
TOF (μs)

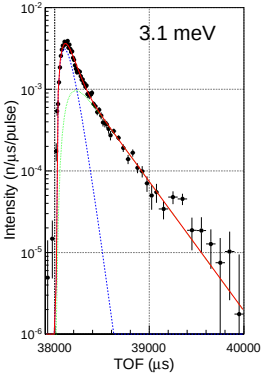
3.1 meV
Intensity (n/μs/pulse)
TOF (μs)

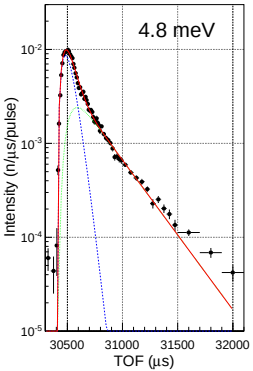
4.8 meV
Intensity (n/μs/pulse)
TOF (μs)

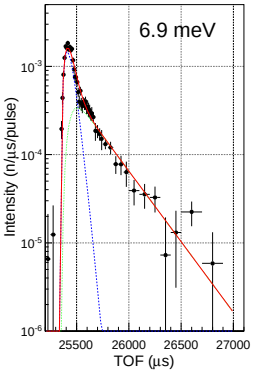
6.9 meV
Intensity (n/μs/pulse)
TOF (μs)

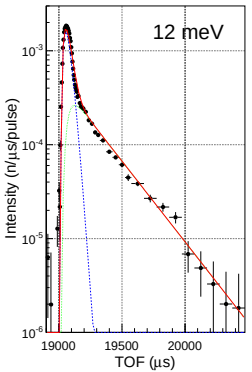
12 meV
Intensity (n/μs/pulse)
TOF (μs)

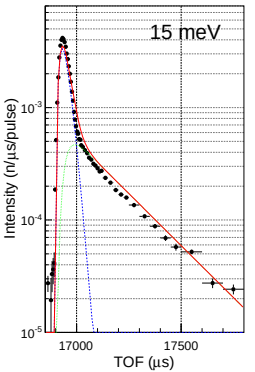
15 meV
Intensity (n/μs/pulse)
TOF (μs)

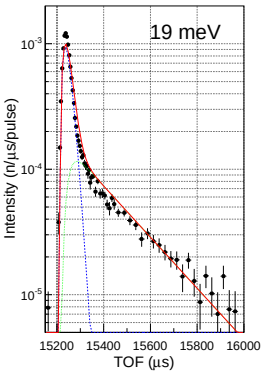
19 meV
Intensity (n/μs/pulse)
TOF (μs)

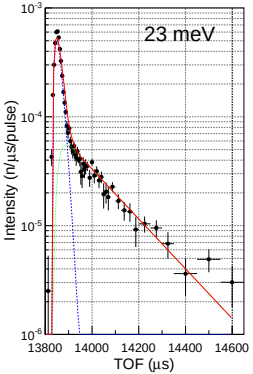
23 meV
Intensity (n/μs/pulse)
TOF (μs)

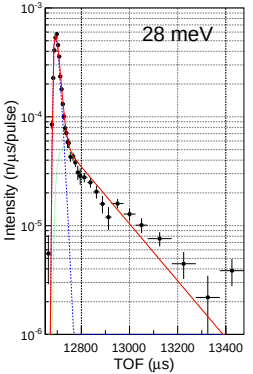
28 meV
Intensity (n/μs/pulse)
TOF (μs)

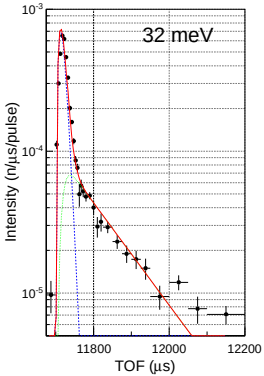
32 meV
Intensity (n/μs/pulse)
TOF (μs)

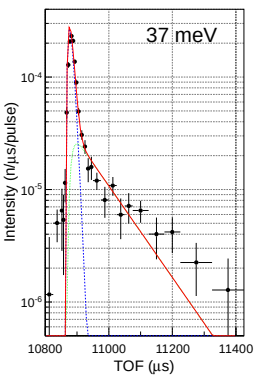
37 meV
Intensity (n/μs/pulse)
TOF (μs)

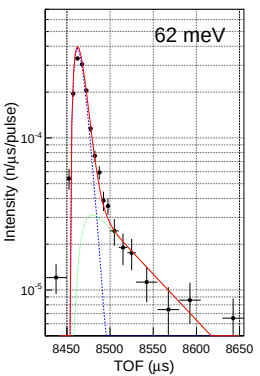
62 meV
Intensity (n/μs/pulse)
TOF (μs)

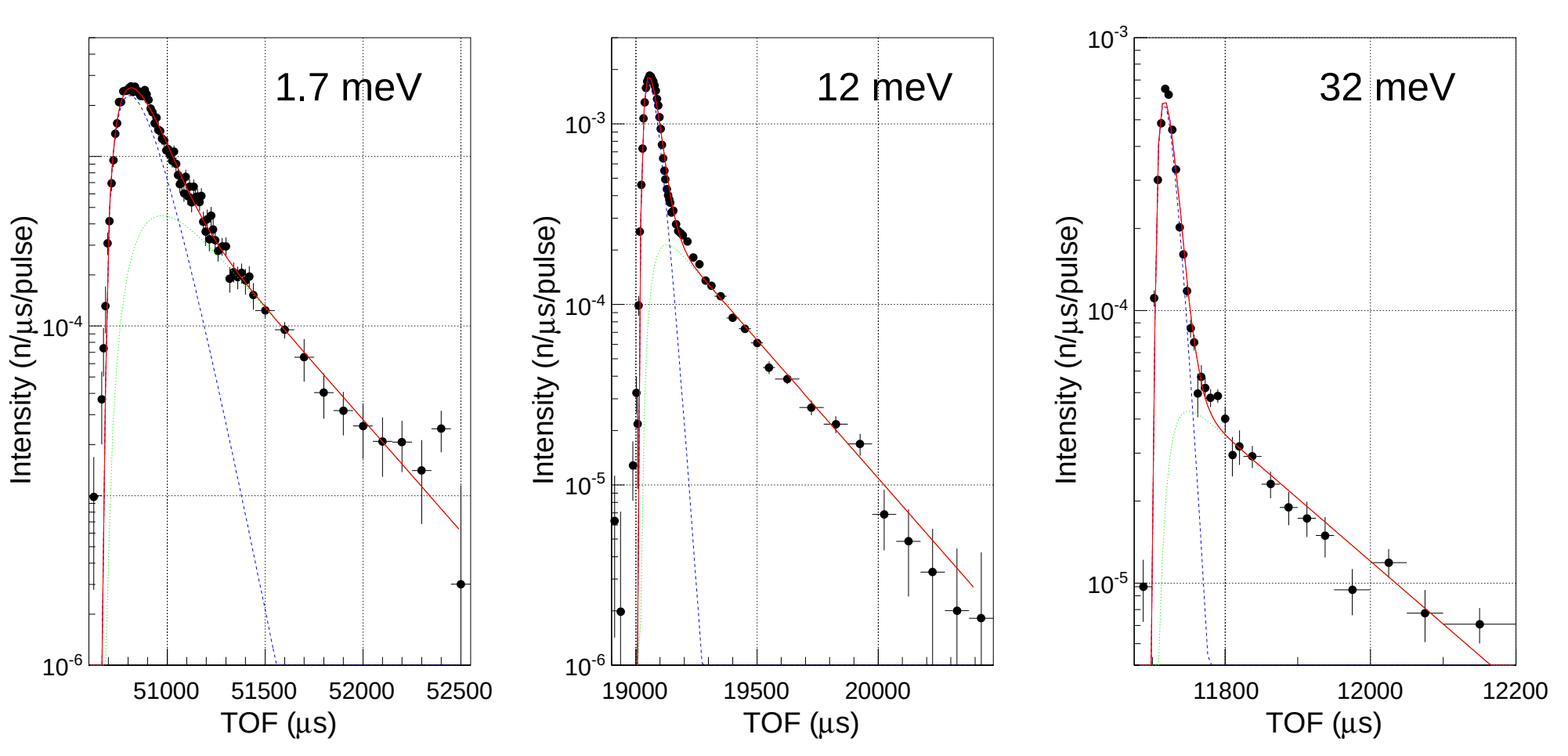
1.7 meV
12 meV
32 meV
Intensity (n/μs/pulse)
TOF (μs)
10^-3
10^-4
10^-5
10^-6
51000
51500
52000
52500
19000
19500
20000
11800
12000
12200

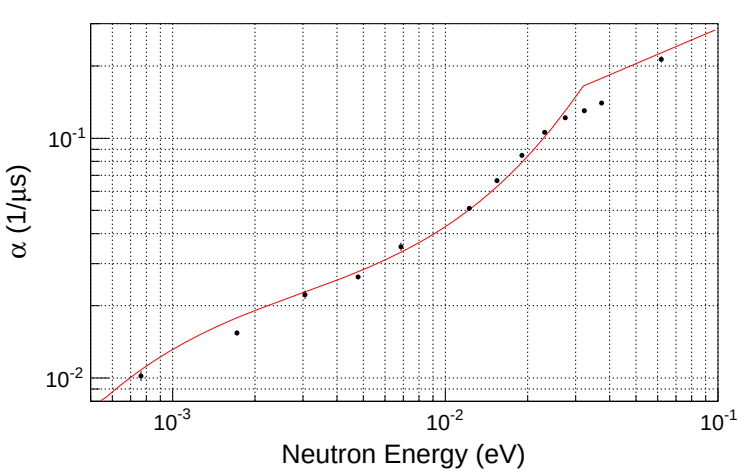
α (1/μs)
10^{-1}
10^{-2}
10^{-3}
10^{-2}
10^{-1}
Neutron Energy (eV)

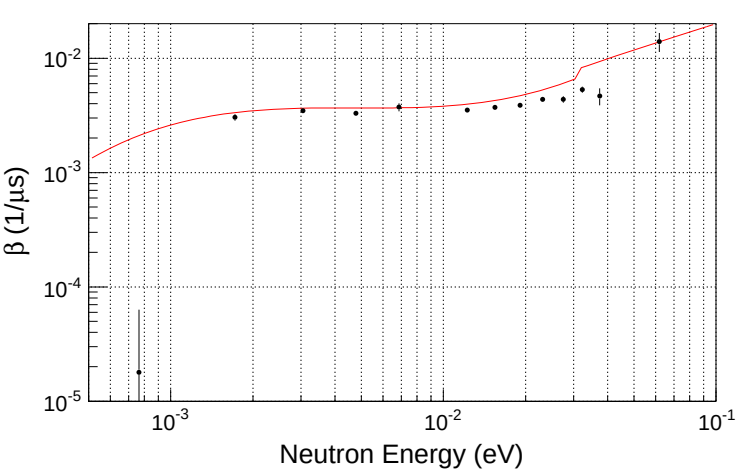
β (1/μs)
10^{-2}
10^{-3}
10^{-4}
10^{-5}
10^{-3}
10^{-2}
10^{-1}
Neutron Energy (eV)

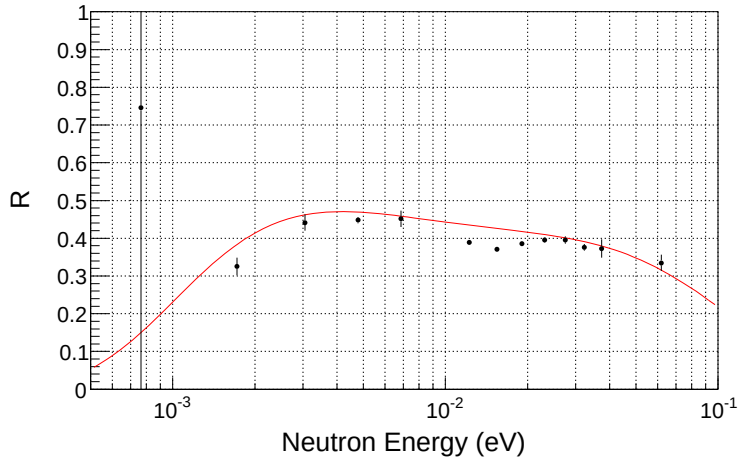
R
1
0.9
0.8
0.7
0.6
0.5
0.4
0.3
0.2
0.1
0
10^{-3}
10^{-2}
10^{-1}
Neutron Energy (eV)

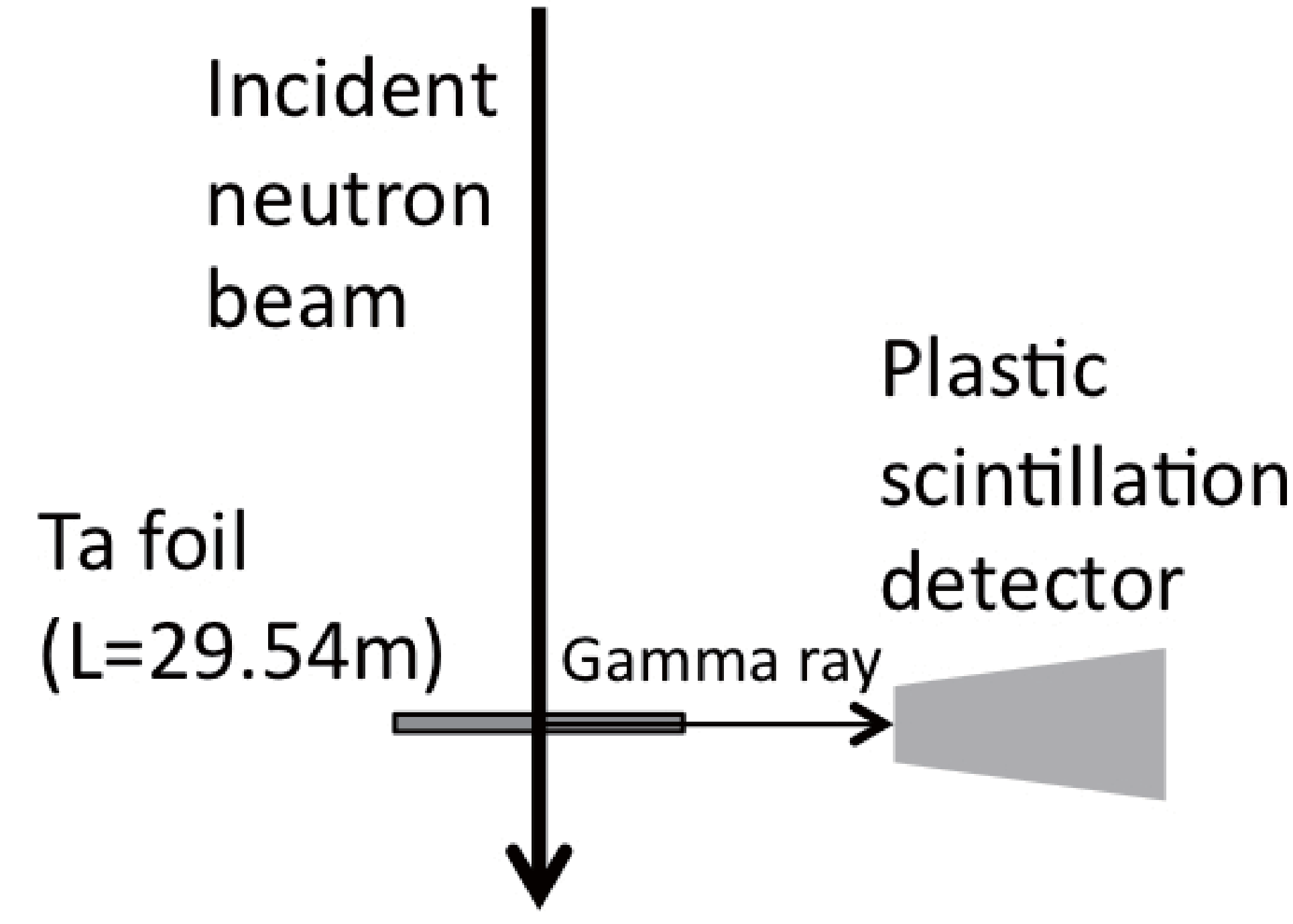
Incident
neutron
beam
Plastic
scintillation
detector
Ta foil
(L=29.54m)
Gamma ray

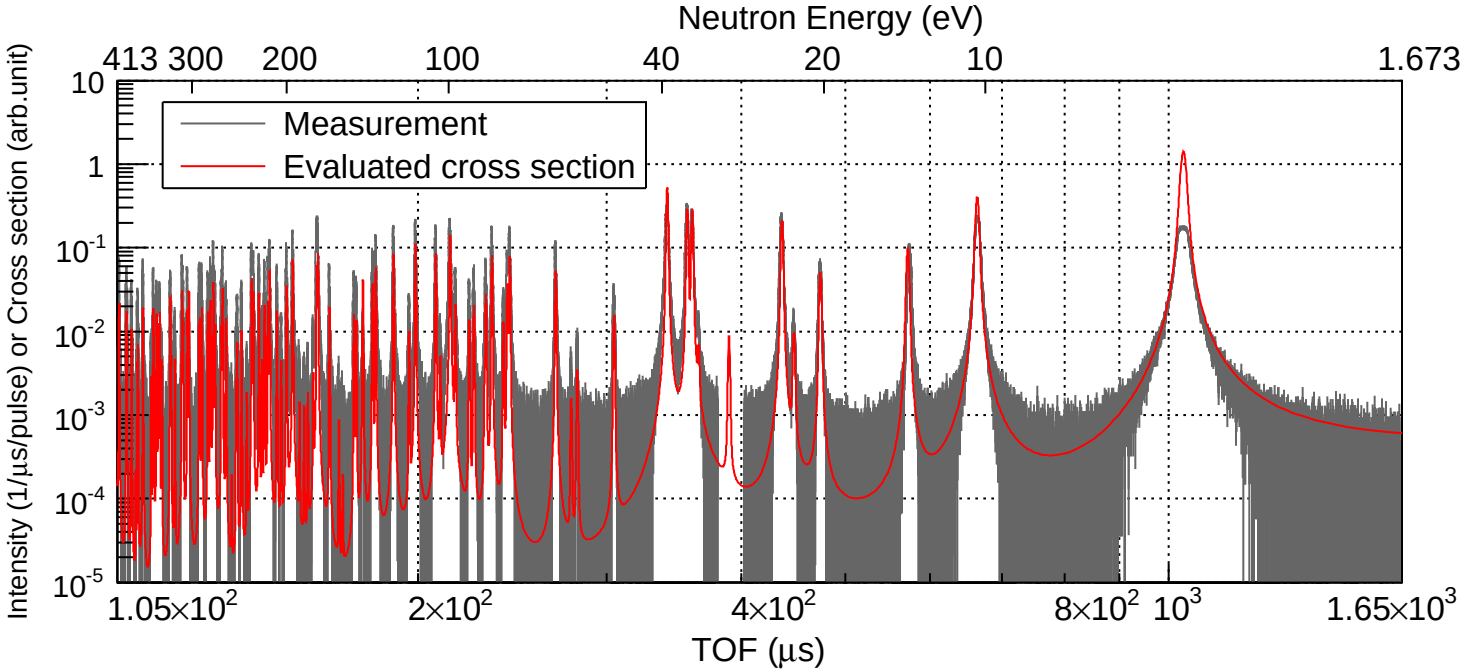
Neutron Energy (eV)
413 300
200
100
40
20
10
1.673
Measurement
Evaluated cross section
Intensity (1/μs/pulse) or Cross section (arb.unit)
10
1
10-1
10-2
10-3
10-4
10-5
1.05×10^2
2×10^2
4×10^2
8×10^2
10^3
1.65×10^3
TOF (μs)

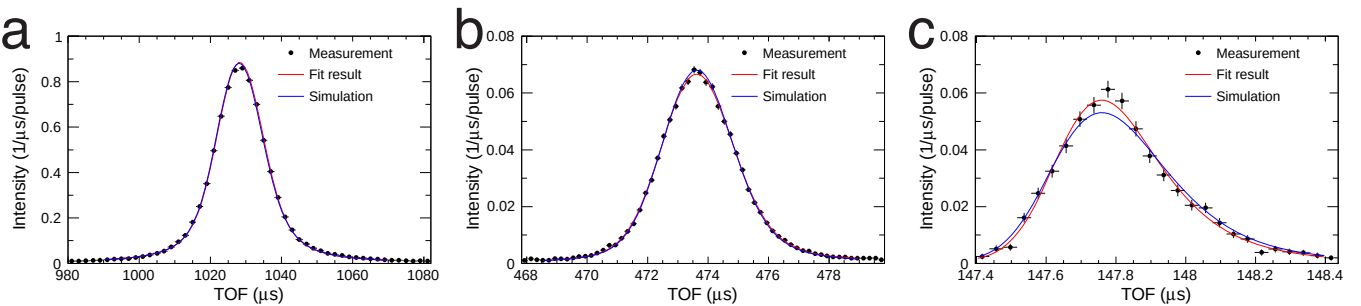
a
b
c
Measurement
Fit result
Simulation
Intensity (1/μs/pulse)
TOF (μs)
0
0.2
0.4
0.6
0.8
1
980
1000
1020
1040
1060
1080
0.02
0.04
0.06
0.08
468
470
472
474
476
478
147.4
147.6
147.8
148
148.2
148.4

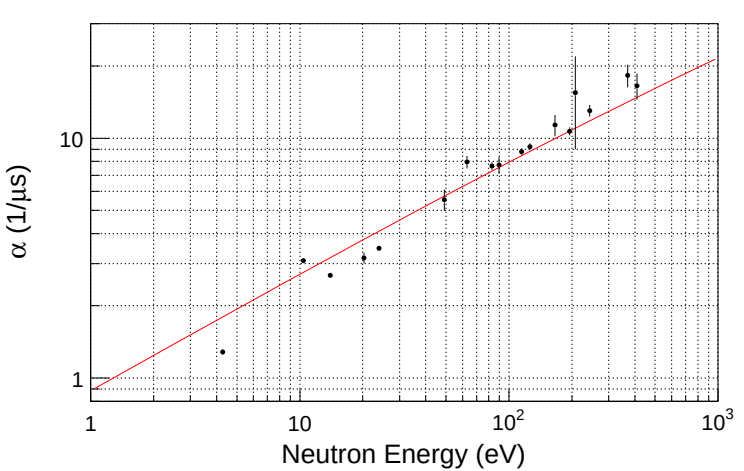
α (1/μs)
10
1
1
10
10^2
10^3
Neutron Energy (eV)

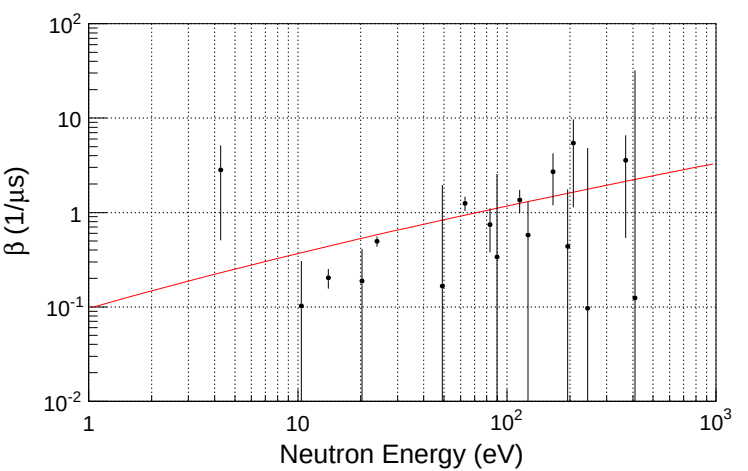
β (1/μs)
10^2
10
1
10^{-1}
10^{-2}
1
10
10^2
10^3
Neutron Energy (eV)

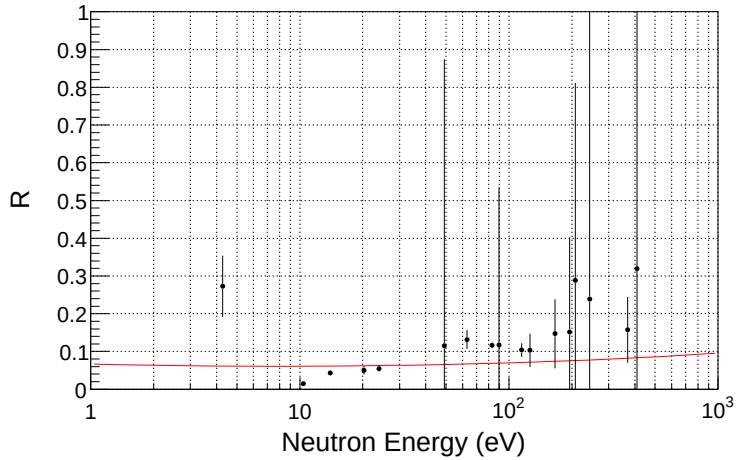
R
1
0.9
0.8
0.7
0.6
0.5
0.4
0.3
0.2
0.1
0
1
10
10^2
10^3
Neutron Energy (eV)

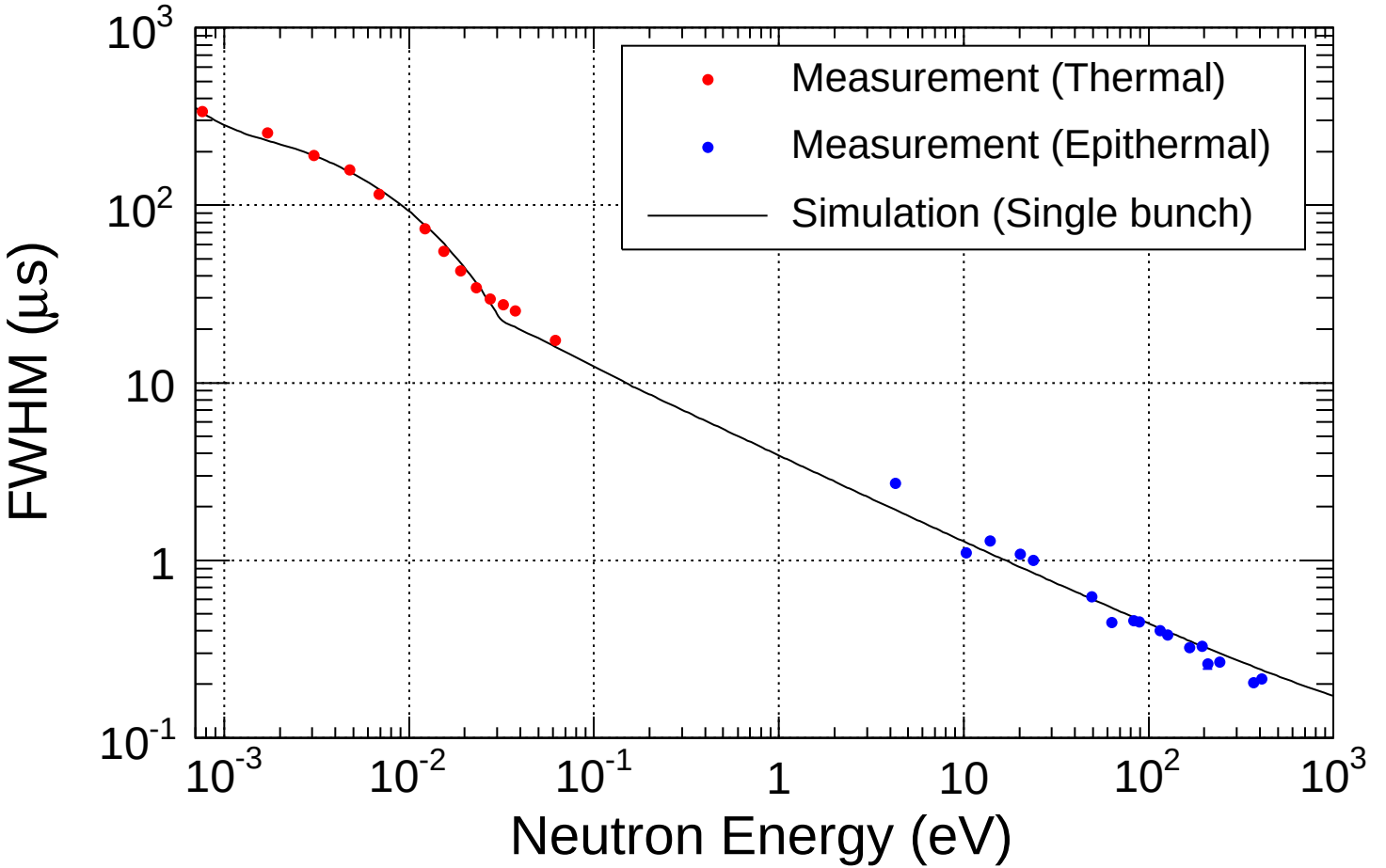
Measurement (Thermal)
Measurement (Epithermal)
Simulation (Single bunch)
FWHM (μs)
Neutron Energy (eV)
10^3
10^2
10
1
10^-1
10^-3
10^-2
10^-1
1
10
10^2
10^3